# Motion Magnification using the Hermite Transform

Jorge Brieva[a], Ernesto Moya-Albor[a], Sandra L. Gomez-Coronel[b], Boris Escalante-Ramírez[c], Hiram Ponce[a] and Juan I. Mora Esquivel[a];

[a] Vision, Machines & Signals Group – Faculty of Engineering,
Universidad Panamericana, México, D.F.
[b] Instituto Politécnico Nacional, UPIITA, Av. IPN No. 2580 Col. La Laguna Ticomán,
Gustavo A. Madero, México D.F. C.P. 07340
[c] Fac. de Ingeniería, Universidad Nacional Autónoma de México, México, D.F.

## ABSTRACT

We present an Eulerian motion magnification technique with a spatial decomposition based on the Hermite Transform (HT). We compare our results to the approach presented in.[1] We test our method in one sequence of the breathing of a newborn baby and on an MRI left ventricle sequence. Methods are compared using quantitative and qualitative metrics after the application of the motion magnification algorithm.

**Keywords:** Automated Respiration Detection, Eulerian Video Magnification, Optical Flow, Hermite Transform

## 1. INTRODUCTION

Eularian motion magnification is a technique that acts like a magnifying lens for visual motion. It can amplify fine motion in a video sequence and allows to perceive movements that are normally invisible or to reveal hidden information. For example it is difficult to visualize small deformations of structures, small movements of a system, etc. The most common applications are related to subtle facial expression recognition[2] and biomedical applications: diagnostic of neoplastic lesions from colorectal exam,[3] to carry out a non-contact detection of cardiac pulse[4,5] or breathing detection mainly in neonates.[6] In fact, magnification can be an auxiliary aid for monitoring vital signals, blood flow and breathing. The principal challenge is to carry out the motion magnification without losing image quality and permit a good localization of the area of interest. Generally, the Eulerian method consists of performing a spatial decomposition and temporal filtering in order to retain the motion components to amplify. Finally, a reconstruction strategy is necessary. Other techniques for motion magnification are described in.[7,8] The first one use the Riesz transform to manipulate the phase in non-oriented sub-bands of an image sequence to produce motion magnification videos, and the second one is based on a quaternionic formulation of the Riesz pyramid. The authors present a new image representation in the spatial domain to avoid spatial wrap-around artefacts present in the frequency domain.

In this paper we present a method using Hermite Transform. We use an Hermite pyramid decomposition and reconstruction strategy in the Eulerian method and then we compare to the traditional Laplacian pyramid decomposition used in.[1] The advantage of a Hermite decomposition is that it uses a Gaussian window and Gaussian derivative operators to extract local information from the image. The Gaussian window is a good model of the overlapping receptive fields found in physiological experiments on the human visual system (HVS). The receptive fields as well as the Gaussian derivative operators in the human eye are spatially local and consist

Send correspondence to J.B.
J.B.: E-mail: jbrieva@up.edu.mx, Telephone: +52 55 5482 1600 Ext. 5267
E.M.A.: E–mail: emoya@up.edu.mx
S.L.G.C.: E–mail: sgomezc@ipn.mx,
B.E.R.: E-mail: boris@servidor.unam.mx,
H.P.: E–mail: hponce@up.edu.mx
J.M.E.: E–mail: 0177169@up.edu.mx

of alternating excitatory and inhibitory regions within a decaying envelope. This allows the Hermite transform to describe a biological model of the measured receptive field data in the HVS.

We test our method in breathing sequence of a newborn baby and on a left ventricle MRI sequence. Methods are compared using quantitative and qualitative metrics after the application of motion magnification algorithm. The rest of the paper is organized as follows: Section 2 describes the Eulerian approach using the Hermite Transform, Section 3 presents the experimental results and discussion of this work, finally Section 4 concludes the paper and presents future work.

## 2. METHODS

In this section we describe the Eulerian motion magnification approach using the Hermite transform (HT) for spatial filtering and we compare with the original method proposed by Wu H.Y. et al.[1] for large amplification factors. First, we present the Hermite transform as a biologically inspired image model and then we use it in the Eulerian motion magnification to perform a spatial filtering and improve the image reconstruction. To compare the two methods, some quantitative and qualitative tests were performed using a baby breathing video and Magnetic Resonance Imaging (MRI) of left ventricle.

### 2.1 The Hermite transform

The Hermite transform (HT) is a special case of the Polynomial transform[9, 10] where the pixel information is analyzed using a window function $v^2(x, y)$ in order to expand the information in terms of a family of polynomials $G_{m,n-m}(x, y)$, which are orthogonal with respect to the window function. From a perceptual point of view, adjacent Gaussian windows separated by twice the standard deviation $\sigma$ represent a good model of the overlapping receptive fields found in physiological experiments.[11] Therefore $v(x, y) = \frac{1}{\sigma\sqrt{\pi}} \exp\left(-\frac{x^2+y^2}{2\sigma^2}\right)$ represents a Gaussian window with a normalization factor that defines a unitary energy for $v^2(x, y)$. The HT is obtained by performing a convolution of the image $L(x, y)$ with the filter functions $D_{m,n-m}(x, y) = G_{m,n-m}(-x, -y)v^2(-x, -y)$ followed by a subsampling $(T)$ as follows (1):

$$L_{m,n-m}(x_0, y_0) = \int_{-\infty}^{\infty} \int_{-\infty}^{\infty} L(x, y) D_{m,n-m}(x_0 - x, y_0 - y) dx dy \tag{1}$$

where $m$ and $(n - m)$ denote the analysis order in $x$ and $y$ respectively, $n = 0, \ldots, \infty$ and $m = 0, \ldots, n$, and $(x_0, y_0)$ represents the positions that conform a sampling lattice $S$.

The associated polynomials $G_{m,n-m}(x, y)$ are defined as (2):

$$G_{m,n-m}(x, y) = \frac{1}{\sqrt{2^n m!(n-m)!}} H_m\left(\frac{x}{\sigma}\right) H_{n-m}\left(\frac{y}{\sigma}\right) \tag{2}$$

where $H_n\left(\frac{x}{\sigma}\right) = (-1)^n \exp\left(-\frac{x^2}{\sigma^2}\right) \frac{d^n}{dx^n} \exp\left(-\frac{x^2}{\sigma^2}\right)$ represents the generalized Hermite polynomials with respect to the Gaussian function (with variance $\sigma^2$). The Hermite filters $D_{m,n-m}(x, y) = D_m(x)D_{n-m}(y)$ are separable because the Gaussian window is rotationally symmetric and can be computed by (3)

$$D_k(x) = \frac{(-1)^k}{\sqrt{2^k k!}} \frac{1}{\sigma\sqrt{\pi}} H_k\left(\frac{x}{\sigma}\right) \exp\left(-\frac{x^2}{\sigma^2}\right) \tag{3}$$

with $k = 0, 1, 2, \ldots, \infty$.

In the practice, the HT may be limited to a few terms because the high order filters analyse high frequencies in the image and successive filters give only very little additional information.

For the discrete case $N$ is the maximum derivative order and $\sigma$ must be related to the spatial scale of the image structures to be analysed. Small windows are better to detect fine details and large windows allow analysing low resolution objects.

Fig. 1(a) shows the Hermite filters for $n = 0, \ldots, 3$ and in Fig. 1(b) we show the Hermite coefficients $L_{m,n-m}$ for frame 141 of the *baby* sequence of the data given in.[12]
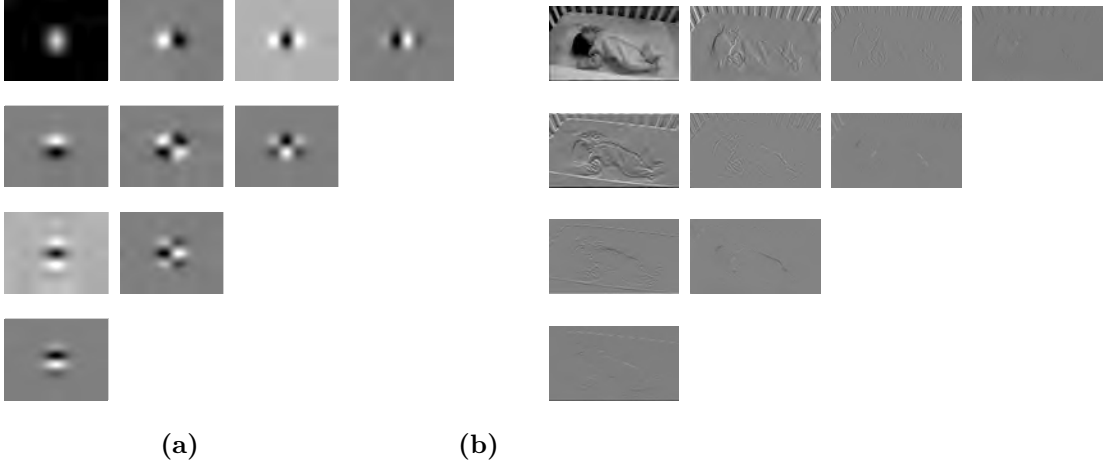
|            |            |
| :--------: | :--------: |
| **(a)**    | **(b)**    |

Figure 1: **(a)** An ensemble of Hermite filters for $m = 0, 1, 2, 3$ and **(b)** Hermite coefficients for frame 141 of the *baby* sequence.[12] The distribution order for the filters and coefficients of Hermite is given by $\begin{bmatrix} 0,0 & 1,0 & 2,0 & 3,0 \\ 0,1 & 1,1 & 2,1 \\ 0,2 & 1,2 \\ 0,3 \end{bmatrix}$.
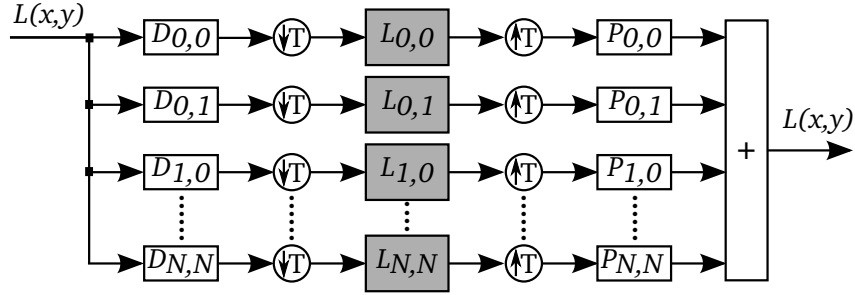


Figure 2: Analysis process of the Hermite transform.

The original image $L(x, y)$ can be reconstructed from the Hermite coefficients by using the reconstruction relation (4):[9]

$$L(x, y) = \sum_{n}^{\infty} \sum_{m=0}^{n} \sum_{(x_0, y0) \in S} L_{m,n-m}(x_0, y_0) \cdot P_{m,n-n}(x - x_0, y - y_0), \tag{4}$$

where $P_{m,n-n}$ are the synthesis filters which are defined by (5):

$$P_{m,n-m}(x, y) = \frac{D_{m,n-m}(x, y)}{V(x, y)}, \tag{5}$$

and $V(x, y)$ is a weight function different from zero for all $(x, y)$, (6):

$$V(x, y) = \sum_{(x_0, y_0) \in S} v^2(x - x_0, y - y_0) \neq 0. \tag{6}$$

In Fig. 2, we show the analysis and synthesis process for the HT.

## 2.2 Eulerian Motion Magnification using the Hermite transform

Let $L(X, t)$ be an image sequence, where $X = (x, y)^\top$ represents the pixel location within a rectangular image domain and $t \in [0, \tau]$ denotes time. Let $W(t) := \left(\delta_x(t), \delta_y(t)\right)^\top$ a vector that defined the displacement $\delta_x(t)$ and

$\delta_y(t)$ of each pixel at position $X$ between an image at time $t$ and another image at time $(t+1)$ in the directions $x$ and $y$ respectively. The observed intensities in the image sequence with respect to the displacement function $W(t)$ can be expressed as $L(X,t) = f\left(X + W(t)\right)$ with $I(X,0) = f(X)$.

The proposal for motion magnification consist of amplifying the displacement function $W(t)$ by a factor $\alpha$ to obtain the synthesized image (7) as expressed below:

$$\hat{L}(X,t) = f\left(X + (1+\alpha)W(t)\right). \tag{7}$$

Expanding $L(X,t) = f\left(X + W(t)\right)$ by a first-order Taylor series we obtain:

$$L(X,t) \approx f(X) + W^T(\nabla f(X)), \tag{8}$$

where $\nabla f(X) := \left(\frac{\partial L(X,t)}{\partial x}, \frac{\partial L(X,t)}{\partial y}\right)^\top$.

Applying a broadband temporal band filter to Eq. (8) where the vector displacement $W(t)$ is retained we get:

$$B(X,t) = W^T(\nabla f(X)). \tag{9}$$

In Eq. (9), $B(X,T)$ represents the motion component of the image sequence $L(X,t)$, so that amplifying $B(X,T)$ by $\alpha$ and adding $L(X,t)$ we have (10):

$$\widetilde{L}(X,t) = L(X,t) + \alpha B(X,t). \tag{10}$$

Combining Eqs. (10) and (8), and assuming that the first–order Taylor series holds, we can demonstrated that the amplification of the temporal bandpass signal is related with to motion amplification (11):

$$\widetilde{L}(X,t) \approx f\left(X + (1+\alpha)W(t)\right). \tag{11}$$

We summarize the steps to compute the Eulerian motion magnification used in this work and proposed by[1] as follows:

1. Carry out a spatial decomposition of the image sequence. This allows decompose the image sequence into different spatial frequency bands that contain spatial frequencies and that are related with different motions.

2. Perform a temporal filtering of the spatial decomposition to retain the motion component of Eq. (9).

3. Amplify the different spatial frequency bands by the $\alpha$ factor.

4. Reconstruct the amplified image sequence through an inverse process to the spatial decomposition of step 1.

5. Add the reconstructed and amplified image sequence to the original image sequence by means of Eq. (10).

In general, the Eqs. (10) and (11) are valid for small motions and for smooth images with slow changes in the image function. However, for images with high spatial frequencies and large motions, the first–order Taylor series approximation of Eq. (8) is not fulfilled.

Therefore a multiresolution strategy is necessary, thus the relation between the amplification factor $\alpha$ and the spatial wavelength $\lambda$ in the current level is given by (12):[1]

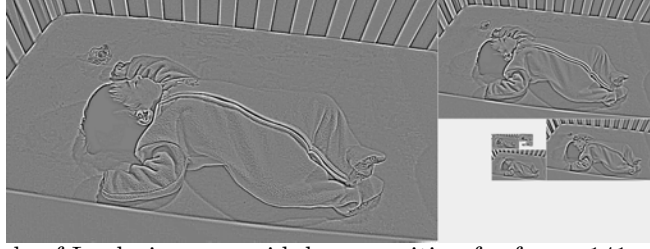$$(1+\alpha)W(t) < \frac{\lambda}{8}, \tag{12}$$

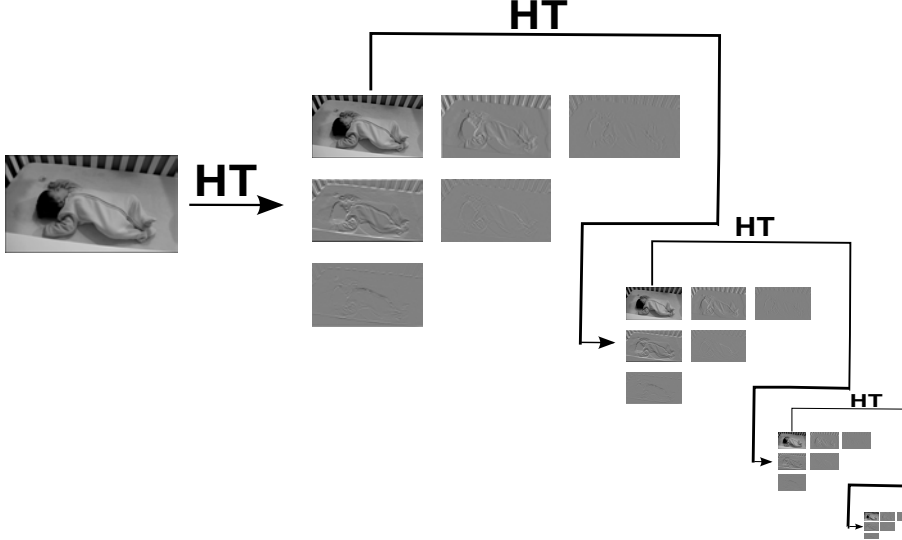Figure 3: An example of Laplacian pyramid decomposition for frame 141 of the *baby* sequence.



Figure 4: An example of Hermite pyramid decomposition for frame 141 of the *baby* sequence.

so that, if $W(t) < \frac{\lambda}{8(1+\alpha)}$ for the current level is not satisfied, a lower amplification factor $\alpha$ is required.

For the spatial decomposition, Wu H.Y. et al.[1] uses a Laplacian pyramid, which it is an image sequence of error, i.e., a difference of two layers of Gaussian pyramid, where each layer of the pyramid can be seen as the response of a bandpass filter, and it represents different spatial frequencies.

In Fig. 3 we show the Laplacian pyramid decomposition for frame 141 of the *baby* sequence using the *matlabPyrTools* package.[13]

Instead of use the Laplacian pyramid decomposition in the spatial filtering, we use the Hermite transform to performs a decomposition of the images taking account the visual features of the image and improve the reconstruction step, this is achieved by the application of Gaussian derivative operators found in psychophysical models of the HVS.[14, 15]

An multiresolution extension of the Hermite transform, that allows analysing objects at different scales, and generates a Hermite pyramid decomposition was presented by Escalante-Ramírez et al.[16] and Silván–Cárdenas et al.[17]

In Fig. (4) we show a Hermite pyramid decomposition with a subsampling factor $T = 2$ and four level of resolution.

To obtain $B(X,t)$ in Eq. (9) a temporal filtering is performed on the pyramidal decomposition $L_*(X,t)$ of the original image (13):

$$B(X,t) = L_*(X,t) * H(X,t) \tag{13}$$

where $*$ represents the convolution operator and $H(X,t)$ is a temporal filter.

Using the Hermite coefficients we can represent the motion component of the image sequence $L(X,t)$ by (14)

$$B_{m,n-m}(X,t) = L_{m,n-m}(X,t) * H(X,t) \tag{14}$$

Applying the inverse Hermite transform to Eq. (14) and combining with Eq. (10) we obtain (15):

$$\widetilde{L}(X,t) = L(X,t) + \alpha \left( \sum_{n} \sum_{m=0}^{n} \sum_{X_0 \in S} B_{m,n-m}(X_0) \cdot P_{m,n-n}(X - X_0) \right) \tag{15}$$

and we can demonstrated that Eq. (15) is related with (16):

$$\widetilde{L}(X,t) = L(X,t) + \alpha \left( W^T(\nabla L(X)) \right). \tag{16}$$

## 3. RESULTS

In this Section we show the results of the Eulerian motion magnification using the approach of Wu H.Y. et al.[1] and the proposal using the Hermite transform as spatial filtering tool. The Laplacian pyramid decomposition and Hermite pyramid decomposition was tested using the *baby* sequence[12] (baby breathing) and using MRI images of left ventricle from *The Cardiac Atlas Project*.[18] In both methods, we used the temporal filtering using the difference of two IIR (Infinite Impulse Response) low-pass filters of the pyramid decomposition $L_*(X,t)$ of the original image as in[1] (17):

$$B(X,t) = \left[ r_1 L_*(X,t) + (1 - r_1)L_*(X,t-1) \right] - \left[ r_2 L_*(X,t) + (1 - r_2)L_*(X,t-1) \right], \tag{17}$$

where $r_1$ and $r_2$ are constant values with $r_1 > r_2$.

We used $r_1 = 0.4$ and $r_2 = 0.05$ and for the spatial wavelength cut–off (Eq. 12) we fixed the value to $\lambda = 16$ as mentioned in.[12] For the Hermite transform the order of expansion was $n = 0, 1, \cdots, 8$ with a Gaussian window of 5x5 elements and a downsampling factor $T = 2$.

The implementation was performed in a Windows–based workstation with an Intel® Xeon® Six–Core Processor at 2.6GHz and 32GB RAM.

The process time was 109.825 seconds for the approach using the Laplacian pyramid and 171.443 seconds using the Hermite transform over the *baby* sequence formed by 301 RBG images of 544x960 pixels. The Hermite transform algorithm uses a non optimized implementation using the convolution operator. There is a fast Hermite transform implementation[17] using only sums and butterfly structures for real-time applications as the proposed by the fast Fourier transform.

### 3.1 Motion Magnification in a Baby Breathing Video

First, we compare the two methods using a baby breathing video. For the amplification factor we used a large value ($\alpha = 50$) to compare the two approaches. In Fig. 5 (first row) we show the images 38, 39, 40 and 41 of the *baby* sequence. Then, in the second row of Fig. 5 we show the results using the algorithm of[12] and in the third row the results using the Hermite transform decomposition. Notice that the images reconstructed using the Hermite transform show less noise than the method proposed by Wu H.Y. et al. We can observe (Fig. 6) that our approach preserve in a better way the important visual structures, e.g., homogeneous regions, edges and textures.

For a visual evaluation of the motion magnification we apply the optical flow algorithm of Moya-Albor et al.,[19] which calculates the displacements of each pixel of two consecutive images in a short period of time. This method uses the Hermite coefficients as local constant constraints into a differential approach.

To calculate the optical flow estimation, the images from the original sequence were used as input in time $t$ and the results of the motion amplification using the two methods were used as imput in time $t + 1$. In Fig. 6 we show the optical flow results to both approaches, the vector fields obtained were filterd for clarity and to show only the vectors above of 0.75 in magnitude.

It is evident from Fig. 6 that Hermite pyramid decomposition allows a better recovery of the displacement field. This is show clearly through the displacement vectors in the amplification motion in the chest of the baby.

Figure 5: Examples of Eulerian motion magnification with $\alpha = 50$ for images 38, 39, 40 and 41 of the *baby* sequence. The first row shows the original images. The second row shows the results using the approach of.[1] The third row shows the results using the Hermite transform.
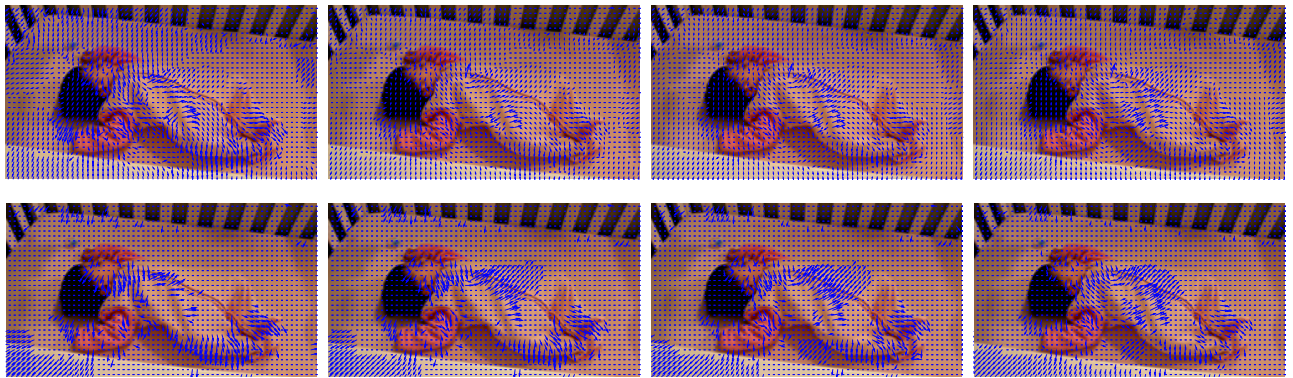


Figure 6: Optical flow results of Eulerian motion magnification with $\alpha = 50$ for images 38, 39, 40 and 41 of the *baby* sequence. The first row shows the optical flow results using Laplacian pyramid decomposition and the second row using the Hermite pyramid decomposition.

The approach of Wu H.Y. et al. doesn't fully recover the vectors related to motion magnification in the chest, we can observe several wrong vectors in the background that correspond to areas with no motion.

Another way to evaluate the quality of the reconstruction (noise and artifacts present in the new sequence) is by calculating the absolute difference between the original image and the motion amplification results. In Fig. 7, we show the difference images using the Laplacian and Hermite pyramid decomposition, where it is observed that in the Laplacian pyramid decomposition there are more discrepancies between the original images and the motion magnification results, some these differences are caused by the breathing movement, but in the areas without motion these differences are caused by artifacts in the motion magnification algorithm.

For a quantitative evaluation of the motion magnification results, we measured the Root Mean Squared ($RMS$) error between the original images in the sequence and the motion results using the Laplacian and Hermite pyramid.
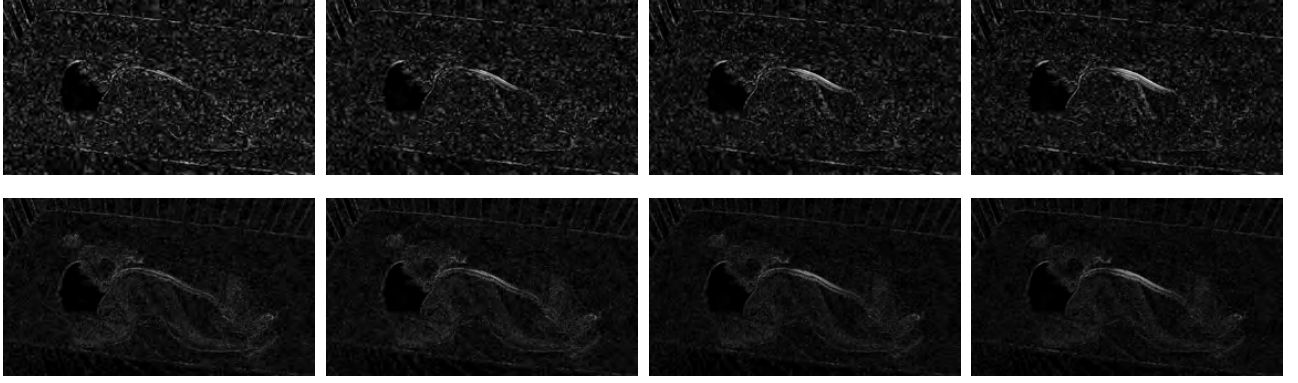
Figure 7: Absolute difference results of Eulerian motion magnification with $\alpha = 50$ for images 38, 39, 40 and 41 of the *baby* sequence. First row shows the difference between the original image and the Laplacian pyramid decomposition result. Second row shows the difference between the original image and the Hemrite pyramid decomposition result.
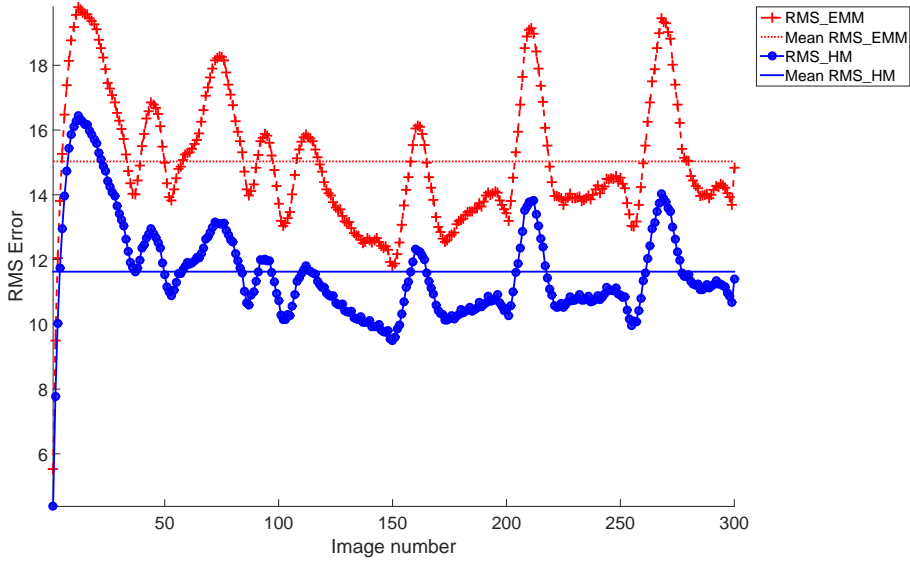


Figure 8: RMS error between the original images in the *baby* sequence and the motion results using the Laplacian (EMM) and Hermite pyramid decomposition (MH)

The RMS error between the $L(X, t)$ and $\widetilde{L}(X, t)$ images is defined by (18)

$$RMS\ error = \sqrt{\frac{\sum_X \left( L(X,t) - \widetilde{L}(X,t) \right)^2}{\mathcal{N}}},\tag{18}$$

where $\mathcal{N}$ is the total number of pixels in the images.

Fig. 8 shows the RMS error throughout the *baby* sequence, where the horizontal axis represents the number of the image and the vertical axis the RMS error. We included in solid line the average RMS error to both methods, where a minimum RMS error for the Hermite transform decomposition is obtained.

Some conclusions can be drawn from Figs. 6 and 7. First, the optical flow is better estimated in the Hermite pyramid decomposition method than Laplacian pyramid approach. While the absolute difference between the original images and the motion amplification results shows the motion areas in both methods, the Laplacian pyramid approach incorporate artifacts in areas without motion that can be observed as highly noisy recon-
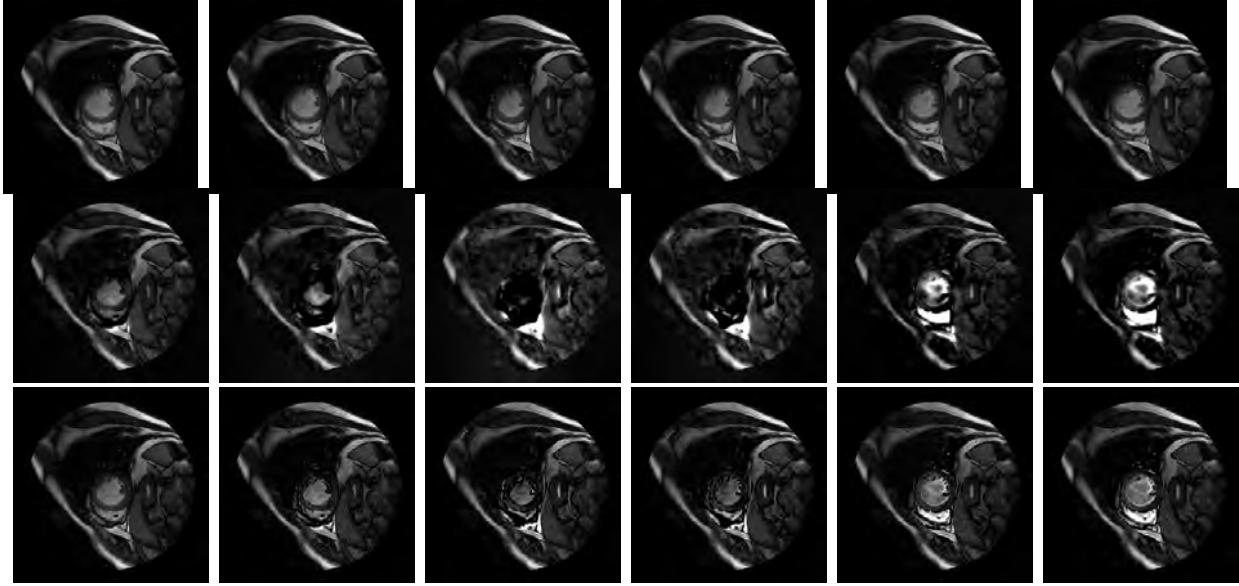
Figure 9: Eulerian motion magnification for a patient with heart failure with infarct at 0%, 5%, 50%, 55%, 85% and 90% of the cardiac cycle, with $\alpha = 25$. First row shows original images. Second row shows the results using the approach of.[1] Third row shows the results using the Hermite transform method.

structed images. Finally, in the quantitative evaluation the Hermite pyramid decomposition method generates a lesser RMS error than the Laplacian pyramid method.

## 3.2 Motion Magnification in MRI images of Left Ventricle

We apply the Laplacian pyramid decomposition and the Hermite pyramid decomposition, in the Eulerian motion magnification approach, to MRI images of a patient with heart failure with infarction. Fig. 9(first row) shows the original images at 0%, 5%, 50%, 55%, 85% and 90% of the cardiac cycle and the results of the Laplacian and Hermite pyramid decomposition are shown in the second an third rows, respectively.

We can see that the motion magnification using the method of Wu H.Y. et al. is too strong and it deforms the structure of left ventricle, whereas the Hermite pyramid decomposition, into the spatial filtering of the Eulerian approach, preserves the visual relevant structures.

## 4. CONCLUSIONS

In this work we have implemented a perceptive approach based on the Hermite transform to Eulerian motion magnification. The Hermite transform is an image representation model that performs a decomposition of the images into relevant visual patterns and mimics some of the more important properties of early vision such as the behavior of retinal ganglion cell, e.g. local processing, and the Gaussian derivative models of receptive fields.

We tested our approach on a breathing sequence of a newborn baby, where we observed that the Hermite approach introduces less noise and better preserves the visual features (less RMS error) as movement (the optical flow is estimated better in the Hermite pyramid decomposition), edges and textures than the Wu H.Y. et al. method.

In MRI left ventricle sequence tests we visually observed that our approach preserves the structures of left ventricle for large amplification factors, whereas the Wu H.Y. et al. method deforms the cardiac structures.

In future work, it is desirable to study other image fatures to optimize temporal filtering to improve extraction of motion components. More generally, we have to test our approach in more real data to study its robustness in different applications and evaluate it's computational performance.

## REFERENCES

[1] Wu, H.-Y., Rubinstein, M., Shih, E., Guttag, J., Durand, F., and Freeman, W. T., "Eulerian video magnification for revealing subtle changes in the world," *ACM Transactions on Graphics (Proc. SIGGRAPH 2012)* **31**(4) (2012).

[2] Park, S. and Kim, D., "Subtle facial expression recognition using motion magnification," *Pattern Recognition Letters* **30**(7), 708 – 716 (2009).

[3] Canales Sevilla, O., Miyagui Maeda, J., Takano Moron, J., and Poquioma Rojas, E., "Utilidad del NBI y Magnificacin ptica en el Diagnstico Diferencial de las Lesiones Neoplsicas y no Neoplsicas Colorrectales en el Per," *Revista de Gastroenterologia del Peru* **30**, 277 – 283 (09 2010).

[4] Balakrishnan, G., Durand, F., and Guttag, J., "Detecting pulse from head motions in video," in [*Computer Vision and Pattern Recognition (CVPR), 2013 IEEE Conference on*], 3430–3437 (June 2013).

[5] Poh, M.-Z., McDuff, D. J., and Picard, R. W., "Non-contact, automated cardiac pulse measurements using video imaging and blind source separation," *Opt. Express* **18**, 10762–10774 (May 2010).

[6] Koolen, N., Decroupet, O., Dereymaeker, A., Jansen, K., Vervisch, J., Matic, V., Vanrumste, B., Naulaers, G., Huffel, S. V., and Vos, M. D., "Automated respiration detection from neonatal video data," in [*Proceedings of the International Conference on Pattern Recognition Applications and Methods*], 164–169 (2015).

[7] Wadhwa, N., Rubinstein, M., Durand, F., and Freeman, W. T., "Riesz pyramids for fast phase-based video magnification," in [*Computational Photography (ICCP), 2014 IEEE International Conference on*], 1–10, IEEE (2014).

[8] Wadhwa, N., Rubinstein, M., Durand, F., and Freeman, W. T., "Quaternionic representation of the riesz pyramid for video magnification," (2014).

[9] Martens, J.-B., "The Hermite transform-theory," *IEEE Transactions on Acoustics, Speech and Signal Processing* **38**(9), 1595–1606 (1990).

[10] Martens, J.-B., "The Hermite transform-applications," *IEEE Transactions on Acoustics, Speech and Signal Processing* **38**(9), 1607–1618 (1990).

[11] Sakitt, B. and Barlow, H., "A model for the economical encoding of the visual image in cerebral cortex," *Biological Cybernetics* **43**(2), 97–108 (1982).

[12] Wu, H.-Y., Rubinstein, M., Shih, E., Guttag, J., Durand, F., and Freeman, W. T., "Web page: Eulerian Video Magnification for Revealing Subtle Changes in the World." `http://people.csail.mit.edu/mrub/evm/` (2012). [accessed 13.05.2015].

[13] Simoncelli, E. P., "MatLab tools for multi-scale image processing." `http://people.csail.mit.edu/mrub/evm/` (2009). [accessed 13.05.2015].

[14] Marr, D. and Hildreth, E., "A theory of edge detection," in [*The Royal Society of London*], B **207**(1167), 187–217 (1980).

[15] Bloom, J. and Reed, T., "A gaussian derivative-based transform," *IEEE Transactions on Image Processing* **5**, 551–553 (mar 1996).

[16] Escalante-Ramírez, B. and Silván-Cárdenas, J. L., "Advanced modeling of visual information processing: A multiresolution directional-oriented image transform based on Gaussian derivatives," *Signal Processing: Image Communication* **20**(9-10), 801–812 (2005).

[17] Silván-Cárdenas, J. L. and Escalante-Ramírez, B., "The Multiscale Hermite Transform for Local Orientation Analysis," *IEEE Transactions on Image Processing* **15**(5), 1236–1253 (2006).

[18] Fonseca, C. G., Backhaus, M., Bluemke, D. A., Britten, R. D., Chung, J. D. D., Cowan, B. R., Dinov, I. D., Finn, J. P., Hunter, P. J., Kadish, A. H., Lee, D. C., Lima, J. A., Medrano-Gracia, P., Shivkumar, K., Suinesiaputra, A., Tao, W., and Young, A. A., "The Cardiac Atlas Project–an imaging database for computational modeling and statistical atlases of the heart.," *Bioinformatics (Oxford, England)* **27**, 2288–2295 (Aug. 2011).

[19] Moya-Albor, E., Escalante-Ramírez, B., and Vallejo, E., "Optical flow estimation in cardiac CT images using the steered Hermite transform," *Signal Processing: Image Communication* **28**(3), 267–291 (2013).